



Cite this: *J. Mater. Chem. C*, 2019, 7, 11014

# UV-sensing organic phototransistor memory devices with a doped organic polymer electret composed of triphenylamine-based aggregation-induced emission luminogens†

Teng-Yung Huang,<sup>‡a</sup> Chia-Hui Chen,<sup>‡a</sup> Chia-Chi Lin,<sup>b</sup> Yu-Jung Lee,<sup>b</sup> Cheng-Liang Liu<sup>id</sup> \*<sup>bc</sup> and Guey-Sheng Liou<sup>id</sup> \*<sup>ad</sup>

This paper reports a UV-sensing organic field-effect phototransistor with a stacked pentacene channel and a doped aggregation-enhanced emission (AIE)-fluorescent electret for potential applications, such as photomemory storage and photodetectors. It is found that the emission of the photoirradiated doped electret (**PA-SMX** and **PI-SMX**) layer can be manipulated at various doping levels, which can be further absorbed by the photoactive pentacene channel. These photogenerated excitons can be separated, and the electrons can be trapped into the electret layer in the presence of gate voltage bias. Therefore, the photoinduced programming and electric field-driven erasing effects of the designed memory device based on doped electrets exhibit optimal photomemory performance with a memory window (MW) of 37.2 V and a reliable retention time over 10 000 s with good cyclic endurance. The photodetection can also be modulated by the illumination power intensity, which reflects a photosensitivity (*S*) of  $1.92 \times 10^6$  and a photoresponsivity (*R*) of  $45 \text{ A W}^{-1}$  for organic phototransistors with the **PI-SM5** doped electret at a photoexcitation intensity of  $720 \mu\text{W cm}^{-2}$  at 365 nm. The photoresponse following the change in the threshold voltage and photocurrent correlate well with the spectroscopic results and provide further understanding and optimization of organic phototransistor memory devices.

Received 3rd July 2019,  
Accepted 13th August 2019

DOI: 10.1039/c9tc03607e

rsc.li/materials-c

## Introduction

Organic memory devices are typically divided into two main categories,<sup>1–5</sup> two-terminal and three-terminal structures, which refer to the structures of organic resistors<sup>6–9</sup> and organic field-effect transistors (OFETs),<sup>10–14</sup> respectively. OFET-type memory devices have received extensive attention because of their non-destructive readout, compatibility with the complementary integrated circuit, and single transistor features combined with light weight, structural flexibility, and simple solution processing of organic/polymeric materials. An electric field is applied to

differentiate between independent stable states from the shifted threshold voltage ( $V_{th}$ ) or modulation of the hysteresis behavior in the OFET transfer curve. A charge trapping/polarization layer is required to achieve transistor memory functionalities, which is conducted by trapping charges in the floating gate/electret and the polarization of ferroelectrics.

The light-receiving OFETs effectively convert light signals into an electric current, which can be amplified in transistor structures.<sup>15–22</sup> With the assistance of photoirradiation, the absorbed light excites the ground state of the organic molecules to produce excitons, which can be separated into holes and electrons at the interfaces under the electric field. The amount of current flow in the accumulation operation of normal OFETs is controlled by the magnitude of the external voltage bias; however, control of the channel conductance in organic phototransistors can be additionally modulated by the absorption of light. This can enable organic phototransistors to develop both functionalities for realizing non-volatile memory for data storage and light sensing for photodetection. In recent years, UV-sensing electronics have drawn great attention for their wide applications, such as fire monitoring, biological analysis, health care, environmental sensors, military uses and space exploration.<sup>23–27</sup> The photoactive channel generally originates

<sup>a</sup> Institute of Polymer Science and Engineering, National Taiwan University, 1 Roosevelt Road, 4th Sec, Taipei 10617, Taiwan. E-mail: gslou@ntu.edu.tw

<sup>b</sup> Department of Chemical and Materials Engineering, National Central University, Taoyuan 32001, Taiwan. E-mail: clliu@ncu.edu.tw

<sup>c</sup> Research Center of New Generation Light Driven Photovoltaic Modules, National Central University, Taoyuan 32001, Taiwan

<sup>d</sup> Advanced Research Center for Green Materials Science and Technology, National Taiwan University, Taipei 10617, Taiwan. E-mail: gslou@ntu.edu.tw

Tel: +886-2-33665315

† Electronic supplementary information (ESI) available: AFM topographies, UV-vis spectra, synthetic routes, inherent viscosity and molecular weight characterization. See DOI: 10.1039/c9tc03607e

‡ These authors contributed equally to this work.

from the organic semiconductor layer; however, the control of UV-sensing photomemory properties is limited because most organic semiconductors with a moderate bandgap result in the absorption in the visible light region.<sup>28</sup> To solve the difficulty, an additional photosensing and charge trapping electret interlayer should be sandwiched between the active semiconductors and gate insulators.<sup>29–38</sup> The introduction of the additional photoactive interlayer film can potentially influence the charge transport and modify the optoelectronic response in the semiconducting channel being operated as a photomemory device and a photodetector. Various materials have been employed for use in the interlayer of organic phototransistor-based memory devices. Han *et al.* reported a novel design for UV-manipulated photonic non-volatile memory devices based on the introduction of CdSe/ZnS core-shell quantum dot monolayers, which displayed remarkable UV-controlled multilevel storage.<sup>29</sup> Optically switchable OFETs featuring a photochromic spirothiopyran (SP) self-assembly monolayer can reversibly photocontrol the carrier density at the interface.<sup>34–37</sup> Our group demonstrated aggregation-enhanced-emission (AEE)-active polyamide for organic phototransistor memory devices because the strong green emission of polyamide under UV-irradiation can be directly absorbed by the pentacene channel, which displayed photoinduced memory behavior.<sup>31</sup> Therefore, an emission peak of the electret interlayer upon UV irradiation that overlaps the absorption peak of organic semiconductors to induce more photoinduced excitons is the key parameter for achieving better memory performance. Of note, tuning the emission in a highly fluorescent aggregation-induced-emission (AIE)-based film *via* doping is a viable strategy for manipulating the generation of excitons of the active semiconducting layer as well as the electrical characteristics (memory properties).

In this work, UV light programming/electrical erasing organic phototransistor memory devices that employ pentacene as the channel and AEE-fluorescent triphenylamine (TPA)-based polymer (PI or PA) doped with an AIE small molecule (SM) as the electret are reported. We engineered the types of blue fluorescent polymers and the doping concentration of the SM. Two polymers with a series of SM doping levels from 1% to 20% (PA-SMX and PI-SMX) were used to tune the emission wavelength near the absorption peak of pentacene for improving the performance of OFET memory devices. Because of the feasible energy transfer from the polymer to the SM in the electret interlayer, highly luminescent materials with a tunable color emission in the film state can be achieved. The photogenerated excitons of pentacene by absorbing the emission light from doped films can be separated, and the charges can be trapped in the electret layer after light-driven programming and a voltage-driven erasing process. The bistable high and low current states refer to the programmed and erased states, respectively, and the devices showed a tunable memory window (MW) and good cyclic switching/significant retention, demonstrating the non-volatile memory characteristics. In addition, the best-performing UV-sensing phototransistors exhibited a maximum photosensitivity ( $S$ ) of  $1.92 \times 10^6$  and a photoresponsivity ( $R$ ) of  $45 \text{ A W}^{-1}$ , which can also effectively detect UV light.

## Experimental section

### Materials

All reagents were obtained from commercial sources and used as received. All the triphenylamine-based compounds with AIE luminogens, including the SMs and two polymers (PA and PI), were prepared according to a previous report,<sup>39,40</sup> and their synthetic routes are shown in Schemes S1–S3 (ESI†). PA and PI polymers were synthesized by direct polycondensation and one-step chemical imidization, respectively.

### Device fabrication

All the organic phototransistor devices adopted a bottom-gate top-contact (BGTC) configuration. The Si/SiO<sub>2</sub> substrate was subjected to wet cleaning steps using deionized water, acetone, and isopropanol. The polymer (PA or PI) was dissolved in DMAc ( $50 \text{ mg mL}^{-1}$ ) and mixed with the SM luminogen at a doping concentration of 1–20 wt%. The filtered solution was spin-coated onto the substrate at 2000 rpm for 60 s, followed by baking at 100 °C for 2 h to obtain the PA-SMX or PI-SMX film (X: SM doping ratio) with a thickness of approximately 80 nm. After transferring the electret-coated samples to a vacuum chamber, the pentacene semiconductor layer was deposited on the electret layer by thermal evaporation at a base pressure of  $3 \times 10^{-6}$  Torr and at a deposition rate of  $2\text{--}5 \text{ \AA s}^{-1}$ . Then, Au electrodes with a thickness of 50 nm were deposited on the pentacene layers through a shadow mask without breaking the vacuum in the chamber. The organic phototransistor with the Au source/drain electrodes had a channel length ( $L$ ) of 50  $\mu\text{m}$  and a channel width ( $W$ ) of 1000  $\mu\text{m}$ .

### Measurements

The thicknesses of the electret films were measured using a surface profiler (Surfcoorder ET3000). The optical absorption and photoluminescence spectra of the PA-SMX and PI-SMX electret films were measured using an Agilent 8453 UV-visible diode array spectrometer and a Horiba Fluorolog-3 spectrofluorometer, respectively. The transistor characteristics were determined in a customized probe station under a N<sub>2</sub> atmosphere by using a Keithley 4200-SCS semiconductor parametric analyzer. A UV lamp (wavelength: 365 nm) was used as the light source, and the actual light intensity was calibrated using a power meter.

## Results and discussion

As illustrated in Fig. 1, the organic phototransistor memory devices were fabricated using a transistor geometry of a bottom gate and top source/drain contact (BGTC), whereas the charge trapping electret layer was deposited by spin coating the AIE-luminescent-doped solution, and the active layer was prepared by thermal evaporation of pentacene on the substrates. Our design principle was that the photoinduced excitons in the semiconductor could be generated with the assistance of the emission-tunable AIE-containing doped electret under UV light illumination, and then could be efficiently trapped into the

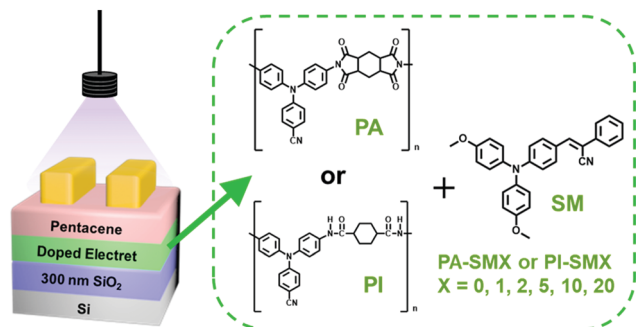


Fig. 1 Schematic diagram of the organic phototransistor memory devices and chemical structures of **PA**, **PI** and **SM** used in the doped electret layer.

electret by applying a reverse voltage bias, resulting in a significant threshold voltage ( $V_{th}$ ) shift. Therefore, the interlayer between the pentacene channel and the multi-functional UV-absorbing/photoluminescence emission/charge trapping electret plays an important role.

The surface topographies of the pristine **PA**, **PI** and **PA-SM5** and **PI-SM5** doped electrets and their corresponding top pentacene organic semiconductor films were first characterized by atomic force microscopy (AFM), as shown in Fig. S1a–d (ESI<sup>†</sup>). All electret films were continuous and relatively uniform (root-mean-square roughness ( $R_{RMS}$ )  $\sim$  0.3 nm) without obvious aggregated clusters. Regardless of the electret-coated substrate, highly regular terrace pentacene structures can be observed (Fig. S1e–h of the ESI<sup>†</sup>). Therefore, the charge trapping ability and memory performance contributed by the morphologies of these two layers can be first excluded.

These luminogens (chemical structures are shown in Fig. 1) based on TPA-containing polymers (**PA** and **PI**) and AIE-active **SMs** were used as doped electret materials, and were prepared according to the synthetic routes shown in Schemes S1–S3 (ESI<sup>†</sup>).<sup>39,40</sup> The inherent viscosity and molecular weight information of **PA** and **PI** is summarized in Table S1 (ESI<sup>†</sup>). These materials are soluble in organic solvents, such as *N*-methyl-2-pyrrolidinone (NMP), *N,N*-dimethylformamide (DMF), dimethyl sulfoxide (DMSO), and *N,N*-dimethylacetamide (DMAc). It was confirmed that the **SM**, **PA** and **PI** materials exhibited the AIE and AEE enhancement phenomena from solution and solid states.<sup>39,40</sup>

The UV-induced emission from the AIE-active-doped electrets covering the pentacene absorption range is a prerequisite for achieving a photoresponse from phototransistor memory cells. Given a specific AEE-active single polymer, the fixed blue light range emission band is a potential obstacle for photon absorption and conversion into free charge carriers within the pentacene layer. Therefore, an organic doping system with effective energy transfer can provide the capability of tuning the emission characteristics and lead to a bathochromic shift, which can possibly match the pentacene absorption range in the hetero-junction structure. In Fig. 2, the pentacene active layer has a wide absorption range based on two main absorption peaks near 581 and 665 nm, and the emission peaks from the pristine UV-excited AEE-active **PA** and **PI** films are at 475 and 436 nm,

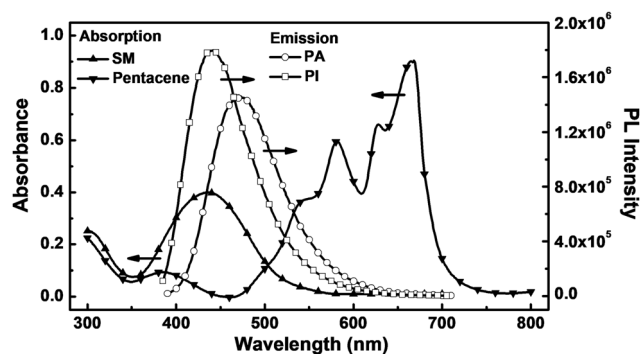


Fig. 2 Absorption spectra of **SM** and pentacene and emission spectra (excited at 365 nm) of **PA** and **PI** thin films.

respectively, which suggest that they do not match each other well with only a small spectral overlap. In our proof-of-concept study, doping **SM** AIE luminogens into a host polymeric material is a viable way to achieve the desirable light emission, thereby producing a UV-photosensitive and charge storage layer. Of note, the existence of a spectral overlap between the emission spectra of the doped electret layer and the photoabsorption of the pentacene layer will be significant for organic phototransistor memory devices. The photophysical properties of doped organic polymer AIE films (**PA-SMX** and **PI-SMX**) with different **SM** doping levels (0–20%) were characterized to investigate the tunable thin film absorption (Fig. S2, ESI<sup>†</sup>) and fluorescence emission through doping. It can be found in Fig. S2 (ESI<sup>†</sup>) that the absorption spectra of doped films closely correspond to a superposition of the spectra of the individual polymer and **SM** and the absorption of the **SM** around 435 nm increases as the **SM** content increases. The tunable emission of **PA-SMX** and **PI-SMX** is illustrated by the evolution of the thin film fluorescence spectra upon changing the **SM** doping ratio (Fig. 3) and the corresponding photographs taken under the illumination of a UV lamp (Fig. S3, ESI<sup>†</sup>). Pristine **PA** and **PI** exhibited one maximum peak at 475 and 436 nm, respectively; however, the fluorescence of the doped **PA-SMX** and **PI-SMX** films revealed a broad and red-shifted emission band. The weak emission at the higher energy region (wavelengths of 400–500 nm) is largely attributed to the emission from the **PA** or **PI** AEE-fluorescent polymer, whereas the main emission peaks could change from 515 to 571 nm and from 546 to 566 nm for **PA-SMX** and **PI-SMX** films, respectively, with increasing **SM** doping concentration that can be attributed to emission from the AIE-active **SM** fluorophore. In the case of the doped **PA-SMX** film, the emission from **PA** decreased, whereas that from the **SM** increased from 0% to 5%. The broad emission profiles for **PA-SM1** and **PA-SM5**, as evidenced by an increase in the full width at half maximum (FWHM) for the emission band, indicate that the presence of the shoulder is attributed to the residual **PA** luminogen and that the emission of **PA** cannot be completely quenched. For **PA** doped with 10% **SMs**, the emission from **PA** was almost completely quenched, whereas that from the **SM** at 564 nm dominated. However, the **PI** emission from 400 to 500 nm was drastically quenched for the doped **PI-SMX** film even at low **SM** doping

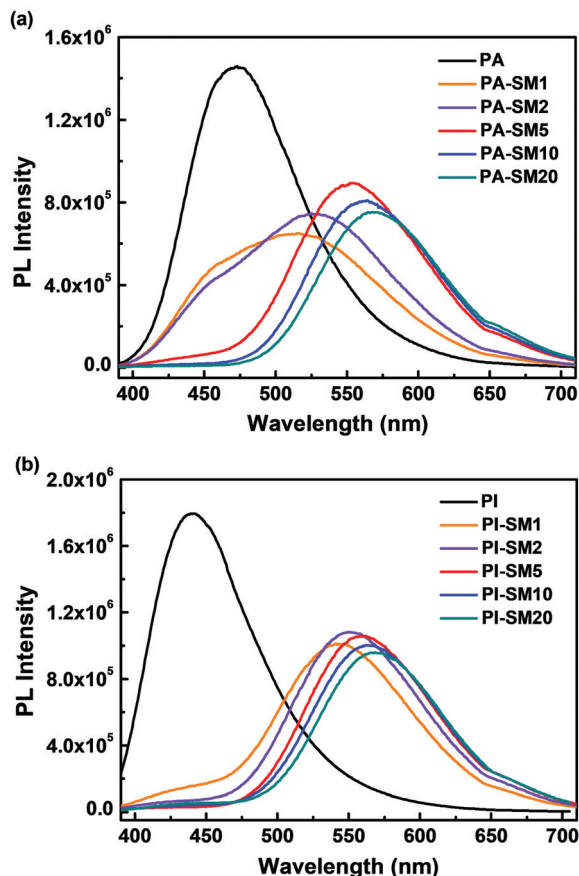


Fig. 3 Emission spectra of (a) PA-SMX and (b) PI-SMX thin films (excited at 365 nm).

concentration. The behaviors in emission spectra verified the energy transfer, which is considered to be a predominant quenching mechanism.<sup>41–44</sup> The absorption spectrum of the SM shows good overlap with the fluorescence emission spectra of the PA or PI polymer in the 400–550 nm wavelength range, implying that the polymers and AIE-active SM can function as an energy transfer pair. For the two combined phases, excitons in the polymer can diffuse to the SM phase and become quenched through energy transfer. The efficiency of energy transfer depends upon the extent of overlap between polymer's emission spectrum and the SM's absorption spectrum. As illustrated in Fig. 2, there is a more significant spectral overlap in the emission of PI/the absorption of the SM relative to the spectrum between PA and SM, which is explained for the strong decrease of emission (at 400–500 nm) of the doped PI-SMX film at a small content of SM. As clearly shown in the photographs, the fluorescence of the doped electret film can be tuned from blue to brown by increasing the SM doping content (Fig. S3, ESI†). Therefore, the doped system from PA (or PI) and the SM can be combined to obtain a large Stokes shift in emission and tunable emission properties, which can be potentially absorbed by the top pentacene semiconducting layer.

The influence of the AIE-luminescent-doped electrets on the charge transport properties of the pentacene layer was investigated *via* field-effect transistor measurements (Fig. 4 and 5).

The pentacene layer provided full coverage over the electret layer, and a stacked hetero-junction could be formed between these two layers. To exclude the operating characteristics of the organic transistor that were attributed to the ambient conditions, electrical measurements were undertaken inside a N<sub>2</sub>-filled glove box. The typical transfer characteristics of the transistor memory devices with the doped electret layer were first measured in the dark. The organic transistor exhibited a p-type channel in the dark. After applying a negative gate voltage ( $V_g$ ) pulse of  $-100$  V with a 30 s duration, which was defined as the erasing process, the transfer curves moved to the negative direction. However, at a positive  $V_g$  of 100 V for 30 s, the transfer curve then moved back to the initial state, which was defined as the programming operation. The memory window (MW), which refers to the variation of the  $V_{th}$  is  $\sim 5.0$  V and  $\sim 10.0$  V for organic transistor memory devices based on PA-SMX and PI-SMX electrets, respectively. This verifies that there is an additional doped electret layer in the pentacene channel, which does not cause any major change in the field-effect transistor operation characteristics; thus, there is no obvious difference between the shifts in dark transfer characteristics measured for the polymer electret with SM doping.

To explore the influence of the electret/semiconductor interface on the light response, pure PA and PI electrets and their doping with SMs were used as UV light-induced charge trapping elements. Fig. 4 and 5 also show the transfer characteristics of organic phototransistor memory devices at a photoexcitation

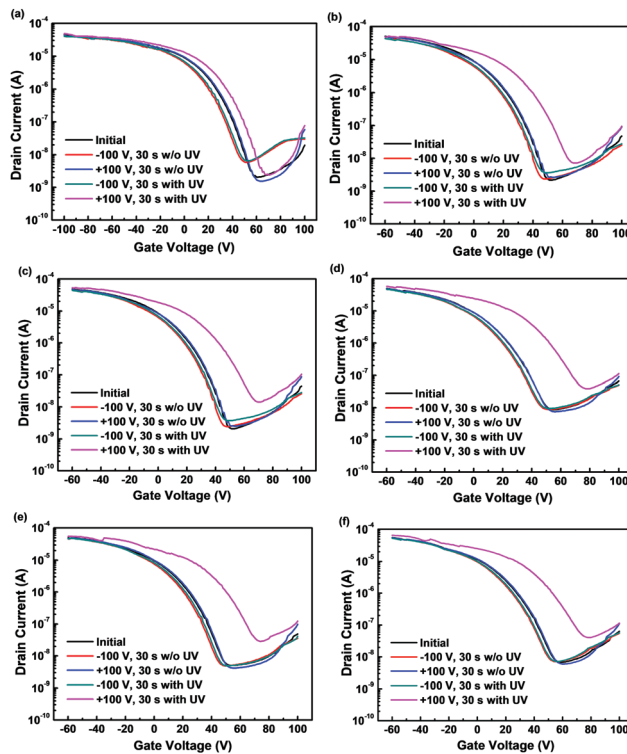


Fig. 4 The transfer characteristics of organic phototransistor memory devices based on (a) PA, (b) PA-SM1, (c) PA-SM2, (d) PA-SM5, (e) PA-SM10 and (f) PA-SM20 in the dark and under UV light illumination (365 nm; 720  $\mu\text{W cm}^{-2}$ ), where  $V_D$  is fixed at  $-60$  V.

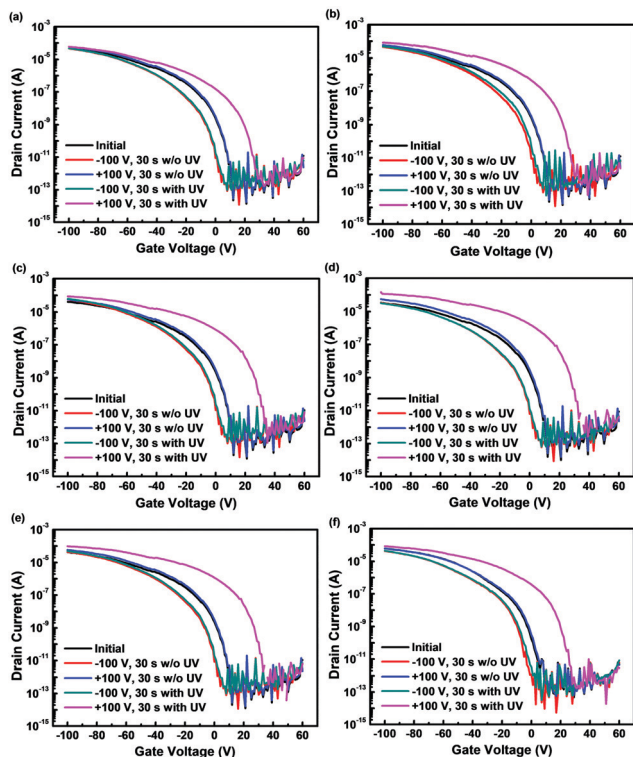


Fig. 5 The transfer characteristics of organic phototransistor memory devices based on (a) PI, (b) PI-SM1, (c) PI-SM2, (d) PI-SM5, (e) PI-SM10 and (f) PI-SM20 in the dark and under UV light illumination (365 nm; 720  $\mu\text{W cm}^{-2}$ ), where  $V_d$  is fixed at  $-100$  V.

intensity of  $720 \mu\text{W cm}^{-2}$  at 365 nm. The statistical results for the MW in the dark and under UV illumination are summarized in Table 1. During programming (100 V) and erasing ( $-100$  V) with UV light illumination, the MW increases to 12.8 V (23.3 V) for pure PA (PI) and 21.2–30.8 V (30.1–37.2 V) for PA-SMX (PI-SMX)-doped electret-based organic phototransistor memory devices, respectively. Compared to the programming process under the dark conditions, the positive backward shift in  $V_{th}$  indicating an additional charge carrier (electrons) trapping ability can be effectively induced with the assistance of UV light illumination. In particular, the observed photoresponse in organic phototransistor memory devices consists of two components: (1) a shift in the programmed  $V_{th}$  towards a more positive direction/a more significant increase in the MW for the device with the AIE-fluorescent polymer electret after doping and (2) a higher MW for the device with the PI-SMX electret compared to that with the PA-SMX electret. The magnitude of the photoinduced MW correlates with the overlap of the emission spectra of the electret upon optical stimulation and the absorption spectrum of the pentacene layer. Therefore, more excitons in the pentacene layer could be dramatically generated in the photomemory device with the doped electret layer (especially for PI-SMX) under UV illumination. The electrons and holes are separated by the application of external  $V_g$ , and the electrons can be further trapped in the electret layer to facilitate the charge transport within the semiconductor channel.

Reliable characteristics, including the data retention capability and cyclic endurance, are important parameters for

Table 1 Photophysical properties and memory characteristics of all the devices

Electret	$\lambda_{max}^a$ [nm]	Emission FWHM [nm]	MW in the dark [V]	MW under UV illumination [V]
PA	475	90	$6.6 \pm 0.2$	$12.8 \pm 0.6$
PA-SM1	515	147	$5.1 \pm 0.2$	$21.2 \pm 0.9$
PA-SM2	525	143	$5.0 \pm 0.1$	$24.0 \pm 0.7$
PA-SM5	555	105	$4.8 \pm 0.1$	$30.8 \pm 1.0$
PA-SM10	564	99	$4.8 \pm 0.3$	$30.0 \pm 0.7$
PA-SM20	571	101	$4.3 \pm 0.2$	$28.8 \pm 0.8$
PI	436	84	$10.6 \pm 0.1$	$23.3 \pm 1.1$
PI-SM1	546	109	$10.4 \pm 0.3$	$30.1 \pm 1.5$
PI-SM2	554	105	$9.6 \pm 0.3$	$35.9 \pm 1.8$
PI-SM5	558	102	$9.8 \pm 0.4$	$37.2 \pm 1.9$
PI-SM10	564	102	$9.5 \pm 0.2$	$32.6 \pm 2.1$
PI-SM20	566	104	$9.5 \pm 0.1$	$30.9 \pm 1.4$

<sup>a</sup> Wavelength at maximum emission (excited by UV light).

nonvolatile memory devices. Fig. 6a shows the charge retention ability of an organic phototransistor memory device with PI-SM5 as a function of time. The programmed (high current) and erased (low current) states were observed after 100 V and  $-100$  V with and without light assistance, respectively. The reading  $I_d$  of these two states was measured at a  $V_g$  of 5 V and  $V_d$  of  $-100$  V. In this case, the current ratio between the programmed and erased states (so-called memory ratio) can be maintained over  $\sim 10^4$  for more than 10 000 s, confirming that the trapped electrons in the doped electret layer are quite stable. The reversible switching behavior was also investigated through the dynamic response of the PI-SM5 electret-based photomemory device with a series of programming ( $V_g = 100$  V, under illumination), reading ( $V_g = 5$  V, in the dark), erasing ( $V_g = -100$  V, in the dark), and reading processes, which refers to the program–read–erase–read (PRER cycles (Fig. 6b)). There was no significant variation in the single response during the programmed/erased cycles, indicating the obtained device with good reversibility and stability.

According to the photoelectric analysis above, the operation mechanism of our organic phototransistor memory devices with the doped AIE-fluorescent electret can be proposed in Fig. 7. During the UV light-assisted programming process (Fig. 7a), the strong fluorescence emission from the electret layer was perfectly absorbed by the top pentacene, and photo-induced excitons (or electron/hole pairs) were generated in the pentacene layer (Fig. 7b). When appropriate positive  $V_g$  was applied to the device, the excitons could be divided into holes and electrons, then, the electrons tunneled from pentacene were trapped into the doped electret layer to achieve charge separation (Fig. 7c). The trapped electrons could effectively increase the concentration of holes within the pentacene channel; consequently, the photogating effect would bring about a positive shift of  $V_{th}$  when the measurement was conducted under UV light illumination. The electrical erasing process can be operated by applying an opposite voltage (negative  $V_g$ ) in the dark, and the electrons can further diffuse back to the pentacene to neutralize the residual holes, which is confirmed by the negatively shifted transfer curves.

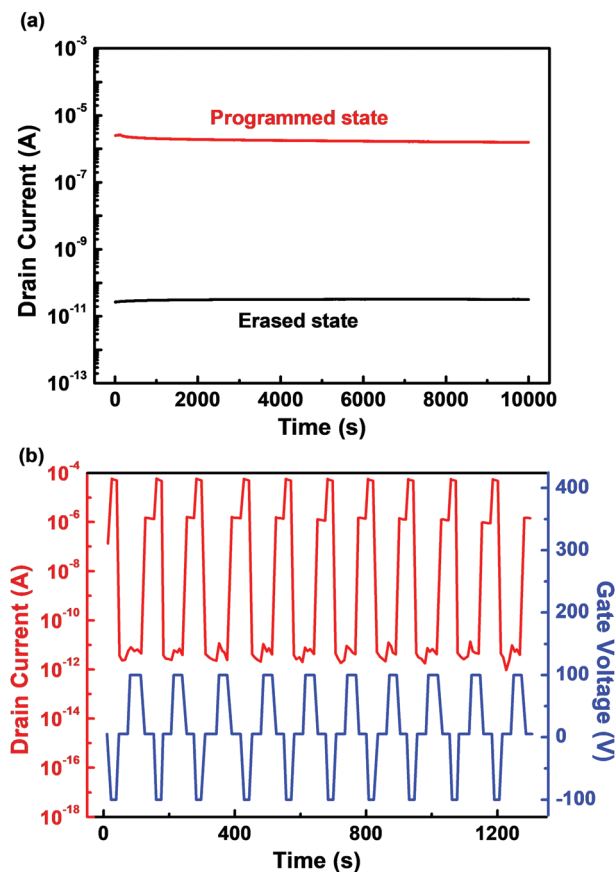


Fig. 6 (a) Retention time characteristics of organic phototransistor memory devices based on PI-SM5 for the programmed state ( $V_g = 100$  V, 30 s) under UV illumination ( $365$  nm;  $720 \mu\text{W cm}^{-2}$ ) and the erased state ( $V_g = -100$  V, 30 s) in the dark, respectively, where  $V_d$  is fixed at  $-100$  V. (b) Endurance cycle test of organic phototransistor memory devices based on the PI-SM5 electret: reading  $I_d$  at  $V_g = 5$  V after programming with  $V_g = 100$  V and UV light exposure and erasing with  $V_g = -100$  V.

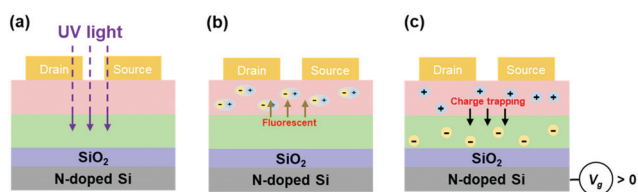


Fig. 7 Schematic diagram showing the operation mechanism of organic phototransistor memory devices: (a) under UV illumination, (b) photoinduced excitons at the pentacene layer, and (c) charge trapping under the reverse bias.

Therefore, the photocurrent could be induced under UV illumination if the photogenerated excitons can efficiently diffuse toward the hetero-junction pentacene/electret interface, then the separated electrons can move to the electret, resulting in a more distinct positively shifted  $V_{th}$  and larger MW compared to the dark programming/erasing conditions.

The performance of the phototransistor with the AIE-fluorescent doped electret was further analysed by quantifying the photodetector at different UV illumination intensities. The

optimized organic phototransistor with the PI-SM5 electret was selected to ensure the photodetection performance. Fig. 8a depicts the modulation curves under dark and illuminated conditions at different illumination powers ( $60$ – $720 \mu\text{W cm}^{-2}$ ) with  $V_g$  sweeping from  $60$  V to  $-100$  V and a fixed  $V_d$  of  $-100$  V. All curves were measured independently. The exposure of the device to light led to an enhanced photocurrent ( $I_d$ ) at the same  $V_g$  ( $10$  V) and positively shifted  $V_{th}$  compared to the device in the dark. This can be attributed to more electrons being trapped from the separation of more photogenerated excitons under illumination. The photocurrent amplitude is highly dependent

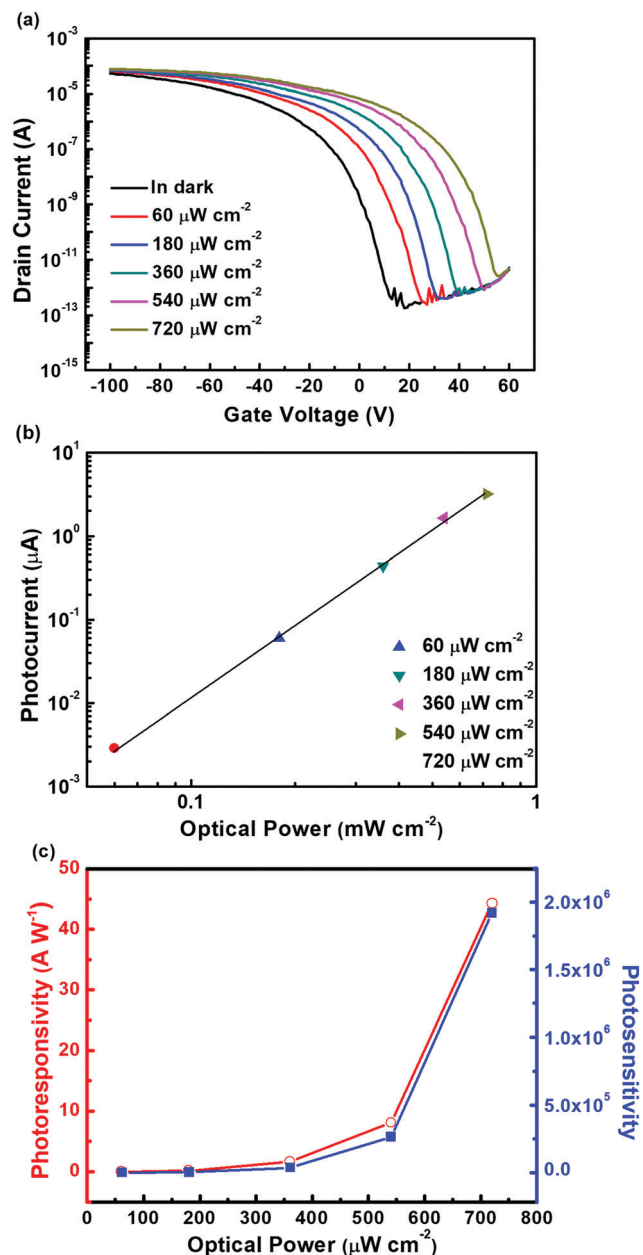


Fig. 8 Organic phototransistor memory devices based on the PI-SM5 electret under UV light illumination: (a) transfer characteristics illuminated under various  $P_{ill}$ ; (b) photocurrent vs. various  $P_{ill}$ ; and (c)  $R$  and  $S$  measured at various  $P_{ill}$ . The  $V_d$  is fixed at  $-100$  V.

on the optical power, and this dependence is usually described by the power law,<sup>45,46</sup>

$$I_d \sim P^k \quad (1)$$

where  $P$  is the optical power and  $k$  is the empirical value. After fitting the measured data to eqn (1),  $k = 2.85$  was obtained (Fig. 8b). This power law relationship further demonstrates that the trapped electrons are responsible for the photogenerated  $I_d$ . Meanwhile, two important parameters were used to assess the performance of the organic phototransistor, namely photosensitivity ( $S$ ) and photoresponsivity ( $R$ ).  $S$  is defined as the ratio of photogenerated current to the dark current and is given as

$$S = \frac{I_{\text{illum}} - I_{\text{dark}}}{I_{\text{dark}}} \quad (2)$$

where  $I_{\text{illum}}$  and  $I_{\text{dark}}$  are the currents under illumination and in the dark, respectively. However,  $R$  is defined as the ratio of photogenerated current to the incident illumination power ( $P_{\text{ill}}$ ). The  $R$  value can be calculated *via* the following equation.

$$R = \frac{I_{\text{illum}} - I_{\text{dark}}}{P_{\text{ill}}} \quad (3)$$

Fig. 8c depicts the dependence of  $S$  and  $R$  on  $P_{\text{ill}}$  at reading  $V_g$  of 10 V. Both the  $S$  and  $R$  increased with increasing  $P_{\text{ill}}$  caused by the additional charge photogeneration. The device exhibits enhanced signal amplification, and the photoresponse is linear to the  $P_{\text{ill}}$ . The maximum values of  $S$  and  $R$  are  $1.92 \times 10^6$  and  $45 \text{ A W}^{-1}$ , respectively, at  $P_{\text{ill}}$  of  $720 \mu\text{W cm}^{-2}$ , implying potential application for organic photodetectors. Thus, our work highlights the use of an organic phototransistor integrated with a doped AIE-fluorescent electret as a promising strategy towards developing organic phototransistors with tailored photomemory and photosensing effects.

## Conclusions

In summary, we developed organic phototransistors containing doped AIE-fluorescent electrets to boost the UV light response for the applications of photomemory storage and photodetectors. The emission wavelength of the AIE-fluorescent **PI** and **PA** doped electret films can be manipulated by incorporation of **SM** AIE luminogens. Effective energy transfer of the doped electret film between the emission of the polymer fluorophore and the absorption of the **SM** fluorophore can be effectively achieved under UV irradiation, which can be utilized in optoelectronic devices. Because of the better spectral matching between the UV-irradiated doped electret emission and absorption of the photoactive pentacene channel, the optimized **PI-SM5** electret-based organic phototransistor device exhibits an enhanced MW of 37.2 V with  $S$  and  $R$  values of up to  $1.92 \times 10^6$  and  $45 \text{ A W}^{-1}$ , respectively, at  $P_{\text{ill}}$  of  $720 \mu\text{W cm}^{-2}$ . Consequently, a novel UV-sensing photomemory device based on organic phototransistor architecture could be obtained using a doped AIE-fluorescent polymer electret, demonstrating that the facile approach in this work is a feasible and judicious design for fabricating high-performance phototransistor memory devices.

## Conflicts of interest

There are no conflicts to declare.

## Acknowledgements

This work was financially supported by the ‘‘Advanced Research Center for Green Materials Science and Technology’’ from the Featured Area Research Center Program within the framework of the Higher Education Sprout Project by the Ministry of Education in Taiwan (108L9006) and the Ministry of Science and Technology in Taiwan (MOST 108-3017-F-002-002, 107-2113-M-002-024-MY3, 107-2221-E-002-066-MY3 and 105-2628-E-008-008-MY3).

## References

- Q. D. Ling, D. J. Liaw, C. X. Zhu, D. S. H. Chan, E. T. Kang and K. G. Neoh, *Prog. Polym. Sci.*, 2008, **33**, 917–978.
- P. Heremans, G. H. Gelinck, R. Muller, K. J. Baeg, D. Y. Kim and Y. Y. Noh, *Chem. Mater.*, 2011, **23**, 341–358.
- S. T. Han, Y. Zhou and V. A. L. Roy, *Adv. Mater.*, 2013, **25**, 5425–5449.
- Z. Y. Wang, L. Y. Wang, M. Nagai, L. H. Xie, M. D. Yi and W. Huang, *Adv. Electron. Mater.*, 2017, **3**, 1600510.
- L. Zhou, J. Y. Mao, Y. Ren, S. T. Han, V. A. L. Roy and Y. Zhou, *Small*, 2018, **14**, 1703126.
- C. L. Liu and W. C. Chen, *Polym. Chem.*, 2011, **2**, 2169–2174.
- Y. Chen, G. Liu, C. Wang, W. B. Zhang, R. W. Li and L. X. Wang, *Mater. Horiz.*, 2014, **1**, 489–506.
- W. P. Lin, S. J. Liu, T. Gong, Q. Zhao and W. Huang, *Adv. Mater.*, 2014, **26**, 570–606.
- C. Y. Wang, P. Y. Gu, B. L. Hua and Q. C. Zhang, *J. Mater. Chem. C*, 2015, **3**, 10055–10065.
- B. M. Dhar, R. Ozgun, T. Dawidczyk, A. Andreou and H. E. Katz, *Mater. Sci. Eng., R*, 2011, **72**, 49–80.
- W. L. Leong, N. Mathews, B. Tan, S. Vaidyanathan, F. Dotz and S. Mhaisalkar, *J. Mater. Chem.*, 2011, **21**, 5203–5214.
- Y. H. Chou, H. C. Chang, C. L. Liu and W. C. Chen, *Polym. Chem.*, 2015, **6**, 341–352.
- C. C. Shih, W. Y. Lee and W. C. Chen, *Mater. Horiz.*, 2016, **3**, 294–308.
- H. E. Lee, J. H. Park, T. J. Kim, D. Im, J. H. Shin, D. H. Kim, B. Mohammad, I. S. Kang and K. J. Lee, *Adv. Funct. Mater.*, 2018, **28**, 1801690.
- Y. L. Guo, G. Yu and Y. Q. Liu, *Adv. Mater.*, 2010, **22**, 4427–4447.
- H. L. Dong, H. F. Zhu, Q. Meng, X. Gong and W. P. Hu, *Chem. Soc. Rev.*, 2012, **41**, 1754–1808.
- K. J. Baeg, M. Binda, D. Natali, M. Caironi and Y. Y. Noh, *Adv. Mater.*, 2013, **25**, 4267–4295.
- Y. Wakayama, R. Hayakawa and H. S. Seo, *Sci. Technol. Adv. Mater.*, 2014, **15**, 024202.
- P. C. Gu, Y. F. Yao, L. L. Feng, S. J. Niu and H. L. Dong, *Polym. Chem.*, 2015, **6**, 7933–7944.

- 20 Y. H. Lee, M. Jang, M. Y. Lee, O. Y. Kweon and J. H. Oh, *Chem*, 2017, **3**, 724–763.
- 21 Y. B. Zhai, J. Q. Yang, Y. Zhou, J. Y. Mao, Y. Ren, V. A. L. Roy and S. T. Han, *Mater. Horiz.*, 2018, **5**, 641–654.
- 22 X. C. Ren, F. X. Yang, X. S. Gao, S. T. Cheng, X. T. Zhang, H. L. Dong and W. P. Hu, *Adv. Energy Mater.*, 2018, **8**, 1801003.
- 23 K.-J. Chen, F.-Y. Hung, S.-J. Chang and S.-J. Young, *J. Alloys Compd.*, 2009, **479**, 674–677.
- 24 L. Sang, M. Liao and M. Sumiya, *Sensors*, 2013, **13**, 10482–10518.
- 25 D. Zheng, H. Fang, P. Wang, W. Luo, F. Gong, J. C. Ho, X. Chen, W. Lu, L. Liao and J. Wang, *Adv. Funct. Mater.*, 2016, **26**, 7690–7696.
- 26 Y. Ning, Z. Zhang, F. Teng and X. Fang, *Small*, 2018, **14**, 1703754.
- 27 W. Ouyang, F. Teng and X. Fang, *Adv. Funct. Mater.*, 2018, **28**, 1707178.
- 28 C. Lee, S. Lee, H. Kim and Y. Kim, *Adv. Electron. Mater.*, 2017, **3**, 1700162.
- 29 S. T. Han, Y. Zhou, L. Zhou, Y. Yan, L. B. Huang, W. Wu and V. A. L. Roy, *J. Mater. Chem. C*, 2015, **3**, 3173–3180.
- 30 Y. J. Jeong, D. J. Yun, S. H. Kim, J. Jang and C. E. Park, *ACS Appl. Mater. Interfaces*, 2017, **9**, 11759–11769.
- 31 S. W. Cheng, T. Han, T. Y. Huang, Y. H. Chang Chien, C. L. Liu, B. Z. Tang and G. S. Liou, *ACS Appl. Mater. Interfaces*, 2018, **10**, 18281–18288.
- 32 Y. J. Jeong, D. J. Yun, S. H. Noh, C. E. Park and J. Jang, *ACS Nano*, 2018, **12**, 7701–7709.
- 33 J. Zhuang, W.-S. Lo, L. Zhou, Q.-J. Sun, C.-F. Chan, Y. Zhou, S.-T. Han, Y. Yan, W.-T. Wong, K.-L. Wong and V. A. L. Roy, *Sci. Rep.*, 2015, **5**, 14998.
- 34 H. T. Zhang, X. F. Guo, J. S. Hui, S. X. Hu, W. Xu and D. B. Zhu, *Nano Lett.*, 2011, **11**, 4939–4946.
- 35 L. A. Frolova, P. A. Troshin, D. K. Susarova, A. V. Kulikov, N. A. Sanina and S. M. Aldoshin, *Chem. Comm.*, 2015, **51**, 6130–6132.
- 36 L. A. Frolova, A. A. Rezvanova, B. S. Lukyanov, N. A. Sanina, P. A. Troshin and S. M. Aldoshin, *J. Mater. Chem. C*, 2015, **3**, 11675–11680.
- 37 H. L. Chen, N. Y. Cheng, W. Ma, M. L. Li, S. X. Hu, L. Gu, S. Meng and X. F. Guo, *ACS Nano*, 2016, **10**, 436–445.
- 38 H. F. Ling, J. Y. Lin, M. D. Yi, B. Liu, W. Li, Z. Q. Lin, L. H. Xie, Y. Bao, F. N. Guo and W. Huang, *ACS Appl. Mater. Interfaces*, 2016, **8**, 18969–18977.
- 39 H. J. Yen, C. J. Chen and G. S. Liou, *Chem. Commun.*, 2013, **49**, 630–632.
- 40 S.-Y. Chen, Y.-W. Chiu and G.-S. Liou, *Nanoscale*, 2019, **11**, 8597–8603.
- 41 A. D. Peng, D. B. Xiao, Y. Ma, W. S. Yang and J. N. Yao, *Adv. Mater.*, 2005, **17**, 2070–2073.
- 42 Y. S. Zhao, H. B. Fu, F. Q. Hu, A. D. Peng, W. S. Yang and J. N. Yao, *Adv. Mater.*, 2008, **20**, 78–83.
- 43 X. Li, Y. Qian, S. Wang, S. Li and G. Yang, *J. Phys. Chem. C*, 2009, **113**, 3862–3868.
- 44 B. J. Scott, M. H. Bartl, G. Wirnsberger and G. D. Stucky, *J. Phys. Chem. A*, 2003, **107**, 5499–5502.
- 45 B. Zheng, Y. Wu, P. Yang and J. Liu, *Adv. Mater.*, 2002, **14**, 122–124.
- 46 S.-C. Kung, W. E. van der Veer, F. Yang, K. C. Donavan and R. M. Penner, *Nano Lett.*, 2010, **10**, 1481–1485.